Structural Engineering and Mechanics, *Vol. 63, No. 4 (2017) 509-519*
DOI: https://doi.org/10.12989/sem.2017.63.4.509

Equivalent static wind loads analysis of tall television towers considering terrain factors of hilltops based on force measurement experiment

Shitang Ke*[1], Hao Wang[1a], Yaojun Ge[2b], Lin Zhao[2b] and Shuyang Cao[2b]

[1]*College of Aerospace Engineering, Nanjing University of Aeronautics and Astronautics, Nanjing 210016, China*
[2]*State Key Laboratory for Disaster Reduction in Civil Engineering, Tongji University, Shanghai 200092, China*

(Received October 18, 2016, Revised May 22, 2017, Accepted June 5, 2017)

Abstract. Wind field in mountainous regions demonstrates unique distribution characteristic as compared with the wind field of the flat area, wind load and wind effect are the key considerations in structural design of television towers situated in mountainous regions. The television tower to be constructed is located at the top of Xiushan Mountain in Nanjing, China. In order to investigate the impact of terrain factors of hilltops on wind loads, firstly a wind tunnel test was performed for the mountainous area within 800m from the television tower. Then the tower basal forces such as bending moments and shear strength were obtained based on high frequency force balance (HFFB) test. Based on the experiments, the improved method for determining the load combinations was applied to extract the response distribution patterns of foundation internal force and peak acceleration of the tower top, then the equivalent static wind loads were computed under different wind angles, load conditions and equivalent goals. The impact of terrain factors, damping ratio and equivalent goals on the wind load distribution of a television tower was discussed. Finally the equivalent static wind loads of the television tower under the 5 most adverse wind angles and 5 most adverse load conditions were computed. The experimental method, computations and research findings provide important references for the anti-wind design of high-rise structure built on hilltops.

Keywords: terrain factors of hilltops; television tower; high-frequency force balance; wind effect; equivalent static wind loads

1. Introduction

As more tall television towers with complex aerodynamic configuration and small damping are built as new city landmarks (Breuer *et al*. 2008), wind load is generally considered one of the main control loads (Feng and Zhang 1997, Kareem *et al*. 1998, Carril *et al*. 2003). To increase the signal transmission distance, many radio and television towers are built on hilltops, where the terrain is complex and the anti-wind safety is the major concern (Li *et al*. 2016).

There are many studies devoted to wind loads and wind-induced vibration of tall television towers, and the earliest anti-wind design for television towers can be traced back to the Eiffel Tower in France. At present the main techniques used for anti-wind analysis are high frequency force balance and aeroelastic model. Kitagawa *et al*. (1997) analyzed the across-wind dynamic response and vortex-induced vibration of television towers using the aeroelastic model. Belloi (Belloli *et al*. 2014) compared the results of aeroelastic model and numerical simulation and found that the wind-induced vibration estimated by numerical simulation contained higher risk due to underestimation. Zhou *et al*. (2010) applied complete quadratic combination (CQC) to random vibration response analysis of Canton Tower considering the effect of cross-term of vibration modes on dynamic response. Yang *et al*. (2016) applied the force measurement experiment to the study of wind loads and surface flow features of towers with triangular lattice form, followed by comparison against the computational fluid dynamic (CFD) result. Other studies involved the use of numerical simulation and field measurements for the estimation of wind loads and wind-induced response in tall television towers (Glanville and Kwok 1995, Pirner and Fischer 1999, Zhang *et al*. 2001). For tall television towers built on hilltops, the existing computations of wind-induced response and equivalent static wind load (ESWLs) rarely consider the most adverse load conditions, i.e., along-wind and across-wind, not to mention the effect of 3D terrain effect on the value range of ESWL of television tower. Relevant national standards (GB50009-2012, ASCE 7-10 2010, AIJ 2004) do not provide a detailed specification on the wind field characteristics on hilltops. The terrain correction factor estimated by the empirical formula for the mountainous region is sometimes the only terrain parameter.

A tall television tower to be built on the hilltop of Xiushan Mountain in Nanjing, China was studied. Both the amplitude and spatial distribution pattern of the wind-induced response of the television tower are dramatically different in mountainous region as compared with the flat area, especially on hilltops. If the terrain factors of the mountainous region are not fully considered, the wind-

*Corresponding author, Associate Professor
E-mail: keshitang@163.com
[a]Ph.D. Student
[b]Professor

ISSN: 1225-4568 (Print), 1598-6217 (Online)

Fig. 1 View of the television tower and the surrounding terrain

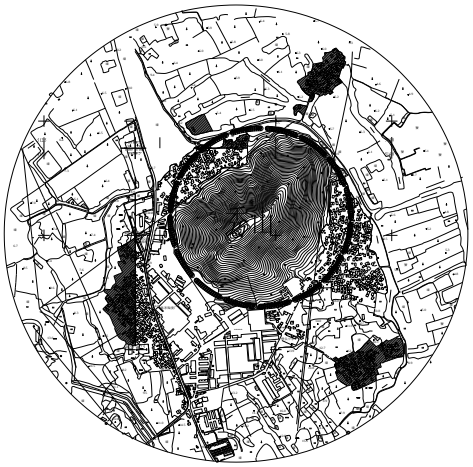

Fig. 2 Sketch of the terrain within 2km from the television tower

Fig. 3 View of the 3D model of the mountainous terrain near the television tower

induced vibration and ESWLs are very likely to be underestimated. However, very few studies have been carried out on the wind effect for television towers in mountainous terrain. Li *et al*. (2011) analyzed the wind-induced response of ultra high-rise buildings in mountainous regions and concluded that the terrain amplification of wind loads was not negligible. Moreover, the amplification ratio of displacement response can reach the maximum of 20%. Therefore, when designing the television towers built on hilltops, high frequency dynamic force measurement and estimation of the distribution pattern of most adverse ESWLs considering the 3D terrain effect will be very important.

Firstly, the wind tunnel test of the mountainous terrain within 800 m from the television tower were performed to obtain the terrain correction factor at the reference height of the tower. Then force measurement experiment was conducted for the rigid body model of the towers using high frequency force balance under different wind angles. The distribution pattern of internal force at the foundation was extracted from the experimental result, and the peak acceleration of the top of structure was investigated. ESWLs under different wind angles, load conditions and equivalent goals were calculated using the improved technique for determining load combination. The effect of terrain factors of hilltop, damping ratio and equivalent goals on wind distribution patterns of the television tower was discussed. Finally ESWL distributions of different layers of the tower were obtained under the 5 most adverse wind angles and 5 most adverse load conditions.

2. Wind tunnel test

2.1 An overview of the project

The television tower to be constructed is situated at the top of the Xianshan Mountain. The relative height of Xianshan Mountain above the flat ground is about 120 m; the main tower stands 87.5 cm high above the ground; the antenna mast is 55 m in length at the top of tower. The total height of the tower is 142.5 m and the relative height from the top of structure to the flat ground is 266.3 m. Designed as a high-rise steel structure with exquisite shape, the television tower is furnished with an outer covering that contributes little to the structural rigidity and strength but increases the frontal area. Since the tower has an exquisite shape and a low damping, it is very sensitive to static and dynamic wind loads. The surrounding terrain and the outer structure of the tower are shown in Fig. 1.

2.2 Simulation experiment on the terrain effect

Fig. 2 shows the topographic contours of the area within 2 km from the television tower (at the elevation of 128.5 m). Xiushan Mountain has a gentle terrain and the adjacent hills are located in the distance. Simulation of the terrain effect was conducted by taking the top of Xiushan Mountain as the center and within a range of about 800m from the center. The simulation model was prepared with a 1:300 scale ratio and the blocking rate was 4.98%. The 3D terrain model of the television tower (Fig. 3) was fabricated by the stack up plastic foam boards. The shape of each plastic foam board depended on the topographic contour lines. Each board had a thickness of 10mm corresponding to 3 m of altitude difference.

A close single circumfluence low velocity wind tunnel

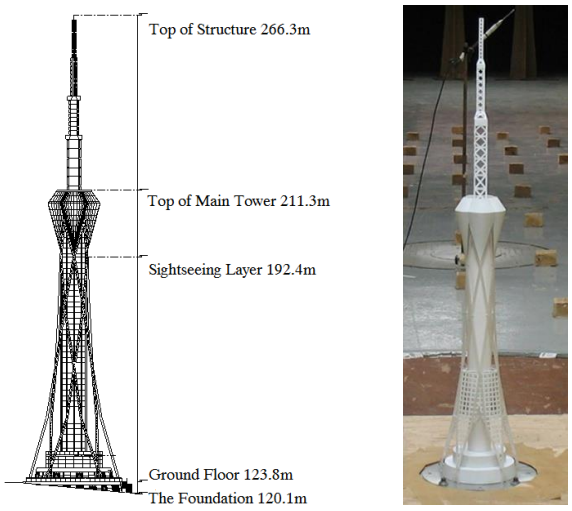

(a) View of the TV tower (b) Rigid body model

Fig. 4 View and experimental model of the television tower

with all-steel structure and tandem arrangement of dual test sections was used for simulation of the terrain effect. The main test section had a width of 3 m and a height of 2.5 m, with continuously adjustable wind speed and 90m/s maximum wind speed. Series 100 Cobra Probe (TFI Corporation, Australia) and the auxiliary equipments were used for wind speed measurement. This probe can provide accurate and efficient wind speed and wind direction measurements under complex wind conditions. The frequency rate of the probe was 500 Hz, and a total of 30000 samples were collected during an interval of 60s.

2.3 Force measurement with high frequency force balance

The experimental model for force measurement was fabricated with lightweight materials and the scale ratio was 1:150. Fig. 4 shows the height of each layer and the rigid body model of the tower.

The model of the tower along with the transmitter room was installed to the rotary table with a diameter of 2.4 m in the test section of wind tunnel. Triangular wedges and roughness elements were arranged at the front of the incoming flow to simulate the atmospheric boundary layer of type B terrain (GB50009-2012 2012). Fig. 5(a) and Fig. 5(b) the comparison between the tested values in wind tunnel and recommended values of GB 5009-2012. Fig. 5(c) shows the measured fluctuating component of the wind speed spectrum along-wind at the reference height and comparison of two empirical spectra. As seen from the Fig. 5, the simulated fluctuating component of the wind speed spectrum satisfied the engineering requirements. Six-component force balance with high frequency response and small inter-component interferences was used. The sampling frequency was 500 Hz, and a total of 30000 samples were collected within an interval of 60s.

3. An improved technique for determining load combinations

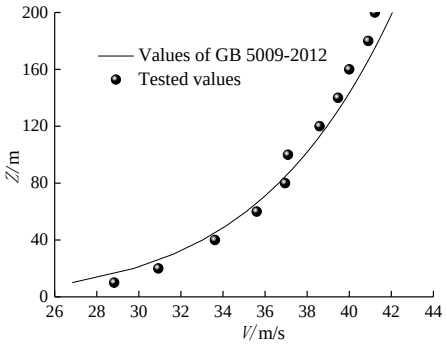

(a) Mean wind profile

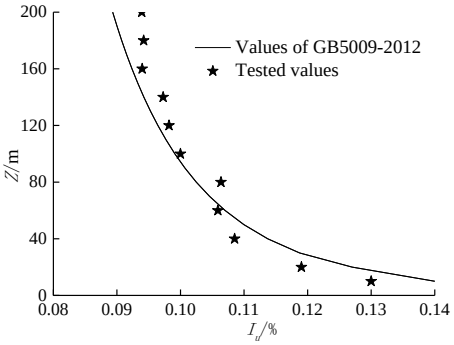

(b) Turbulence intensity profile

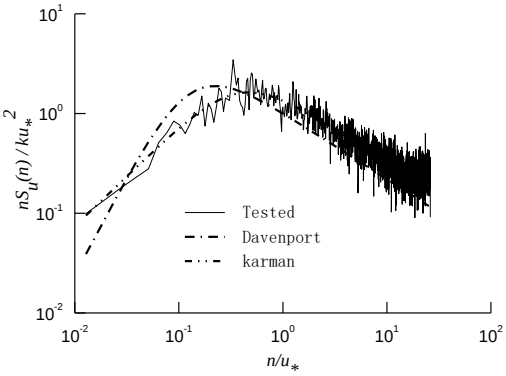

(c) fluctuating component of the wind speed spectrum

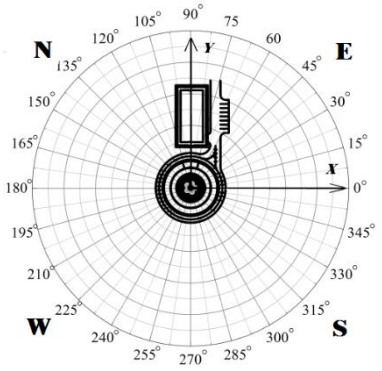

(d) Coordinate system for representing a force

Fig. 5 Wind field characteristics for category B terrain

3.1 Mechanical model

The computational model of the tower was simplified into a series-connected multi-mass system, for which the motion equation under wind loads is expressed as

$$M\,\ddot{\mathrm{x}}(t)+C\,\dot{\mathrm{x}}(t)+K\,\mathrm{x}(t)=F(t) \tag{1}$$

where M, C and K are mass, damping and rigidity matrices of the tower structure, respectively; $F(t)$ is excitation vector of external wind loads:

$$\mathrm{x}=\left\{x_1,x_2,\ \ ,x_n,y_1,y_2,\ \ ,y_n,\theta_1,\theta_2,\ \ ,\theta_n\right\}' \tag{2}$$

where x, y, θ is the translational vectors of the n-layered tower structure along X and Y axis and the rotational vector around z axis, respectively. The subscripts represent different layers, and

$$x(t)=\sum_j \varphi_j \xi_i(t) \tag{3}$$

where φ_j is the j-th order vibration mode vector. For most high-rise buildings, only three lower order vibration modes, namely, horizontal displacement along X and Y axis and rotation around Z axis, have a decisive impact on wind-induced vibration of the structure (Simiu and Scanlan 1978). Based on the assumption that all these three vibration modes are linear, there is

$$f_i=C_{js}\frac{M_y(t)}{H}-C_{jy}\frac{M_x(t)}{H}+\alpha C_{j\theta}M_\theta(t) \tag{4}$$

where $M_x(t)$, $M_y(t)$ and $M_\theta(t)$ are the bending moments of the foundation along X and Y axis and torsional moment of the foundation along Z axis, respectively; α is the adjustment factor depending on the distribution pattern of $f_\theta(z_i,t)$. When $f_\theta(z_i,t)$ is uniformly distributed along the height, the adjustment factor is 0.5 (Ke *et al*. 2012). For buildings with non-coupled vibration modes, only one term is included in the generalized force, while the other two terms are zero.

3.2 Computation of wind-induced response

$M_x(t)$, $M_y(t)$ and $M_\theta(t)$ were all measured with a high frequency force balance. After decoupling, the motion equation under the generalized coordinate system can be solved in the frequency domain. Generalized force after centralization can be used to obtain the fluctuating component of stress response. Power spectrum under the generalized coordinate system is derived from the transfer function

$$S_{z_j}(\omega)=\left|H_i(\omega)\right|^2 S_{f_j}(\omega) \tag{5}$$

$$\left|H_i(\omega)\right|^2=1/\{k_i^2\left\{\left[1-\left(\omega/\omega_i\right)\right]^2+\left(2\omega\zeta_j/\omega_j\right)^2\right\}\} \tag{6}$$

$$\begin{aligned}S_{f_j}(\omega)=\{&C_{jx}{}^2S_{M_y}(\omega)+C_{jy}{}^2S_{Mx}(\omega)\\&+\alpha^2H^2C_{jiy}{}^2S_{M_v}(\omega)\\&+2\alpha HC_{jx}C_{j\theta}\,\mathrm{Re}\left[S_{M_vMij}(\omega)\right]\\&-2\alpha HC_{jx}C_{j\theta}\,\mathrm{Re}\left[S_{MiMij}(\omega)\right]\\&-2C_{jx}C_{jy}\,\mathrm{Re}\left[S_{MiMy}(\omega)\right]\}/H^2\end{aligned} \tag{7}$$

In the generalized force power spectra, S_{Mx}, S_{My}, $S_{M\theta}$, S_{MxMy}, $S_{MxM\theta}$ and $S_{MyM\theta}$ are the auto power spectra for the bending moments along X and Y axis, torsional moment along Z axis and their cross power spectra. Re is the real part of the cross power spectra. These power spectra can be computed from the force measurements. The root mean square acceleration and mean square accelerations are given by

$$\sigma_{\xi_j}{}^2=\sigma_{f_i}{}^2\left(1+[S_{f_j}(\omega)\pi\omega_i]/(\sigma_{f_j}{}^2 4\zeta)\right)/k_i^2 \tag{8}$$

Only considering the first three modes and for small-damping structure with sparse natural frequency, the cross-term of vibration modes can be omitted. Therefore, the mean square displacement of the highest point of the structure can be calculated by using the SRSS technique that degenerates from the CQC technique

$$\sigma_x=\left[\sum_{i=1}^{3}\left(C_{jx}\sigma_{\xi_j}\right)^2\right]^{1/2} \tag{9}$$

$$\sigma_y=\left[\sum_{i=1}^{3}\left(C_{jy}\sigma_{\xi_j}\right)^2\right]^{1/2} \tag{10}$$

$$\sigma_\theta=\left[\sum_{i=1}^{3}\left(C_{j\theta}\sigma_{\xi_j}\right)^2\right]^{1/2} \tag{11}$$

Mean wind-induced vibration can be solved by the mode decomposition technique

$$\begin{aligned}E\left[\xi_i(t)\right]&=\int_{-\infty}^{\infty}E\left[f_i(t-\tau)\right]h_j(\tau)d\tau\\&=E\left[f_i(t)\right]\int_{-\infty}^{\infty}h_j(\tau)d\tau=E\left[f_i(t)\right]H_j(0)\\&=\frac{1}{k_i}E\left[f_i(t)\right]\end{aligned} \tag{12}$$

where E is mathematical expectation. With the mean generalized coordinates obtained, mode superposition is performed to calculate the mean wind-induced vibration (Ke *et al*. 2014).

3.3 Combination method of ESWLs

By referring to the computation of equivalent wind excited vibration force, ESWLs are given by mode decomposition

$$P_{eq}(t)=Kx(t)=\sum_j K\varphi_i\xi_j(t)=\sum_j \omega_j{}^2M\varphi_i\xi_j(t) \tag{13}$$

This equation deals with static mechanics, with $P_{eq}(t)$ equivalent to time series of ESWLs, then

$$P_{eq}(\mathrm{t})=\sum_j A_j\,\xi_J(\mathrm{t}) \tag{14}$$

Suppose that maximum total displacement and maximum displacement of each vibration mode have equal occurrence probability, and let μ be the assurance factor.

Thus the corresponding ESWLs can be expressed by Eq. (15). On this basis, ESWLs of each layer of the tower under different wind angles are computed for use in structural design

$$P_{eq} = Kx_{\max} = \sum_j A_j \bar{\xi}_j + \mu \left[\sum_i \left(A_j \sigma_{\xi_i} \right)^2 \right]^{1/2} \tag{15}$$

When calculating ESWLs under the same load conditions, the forces acting along the two primary directions and the torsional moment acting around the center-of-mass axis (secondary direction) are considered. However, the wind loads in these three directions will not reach the maxima simultaneously. Loads are combined in the secondary direction based on empirical coefficient, assuming that the response in two directions conform to the 2D normal distribution. Then the probability contours of the response, estimated from joint probability distribution, compose an ellipse, expressed as

$$x^2 + 2\rho xy + y^2 = c \tag{16}$$

where x and y are normalized random variables; ρ is the coefficient of correlation between x and y; c is a constant depending on the probability level. With the response extremum $\hat{x}$ calculated along a primary direction, accompanying response in the secondary direction can be obtained by a correlation analysis:

$$y_e = \bar{y} \pm |\rho| (\hat{y} - \bar{y}) \tag{17}$$

where $\bar{y}$ is the mean response in secondary direction; $\hat{y}$ is response extremum in secondary direction and its value is related to the correlation coefficient. $\hat{x}_{\max}$ and $\hat{y}_{\max}$ are the response maxima in the primary and secondary directions under all wind angles, respectively. Thus for these two directions, the combination coefficients are denoted as $\hat{x}/\hat{x}_{\max}$ and $\hat{y}/\hat{y}_{\max}$, respectively.

4. Result of simulation of terrain effect and analysis

4.1 Terrain correction factor for the hilltop

Simulation of the terrain effect was intended for measuring the wind speed time course of incoming flow from the far end and that of the reference height (tower top). The ratio of mean wind speed at the reference height to that of the incoming flow from the far end at the same height was defined as terrain correction factor for the hilltop considering the wind pressure height coefficient under the terrain effect

$$\Delta S = \frac{U(z_{\text{ref}})}{U_0(z)} \tag{18}$$

where $U(z_{ref})$ is the mean wind speed at the reference height; $U_0(z)$ is the mean wind speed of the incoming flow from the far end at the same height.

4.2 Result analysis

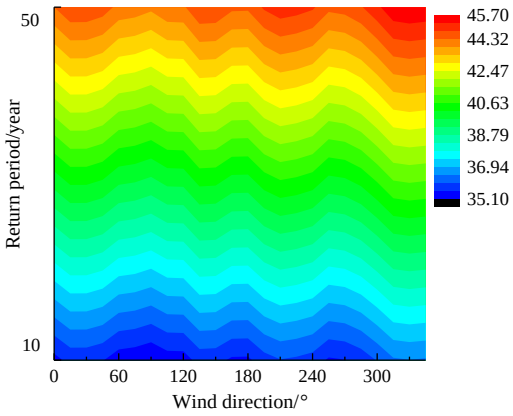

Fig. 6 Wind speeds at the reference height for the return period from 10 to 50 years

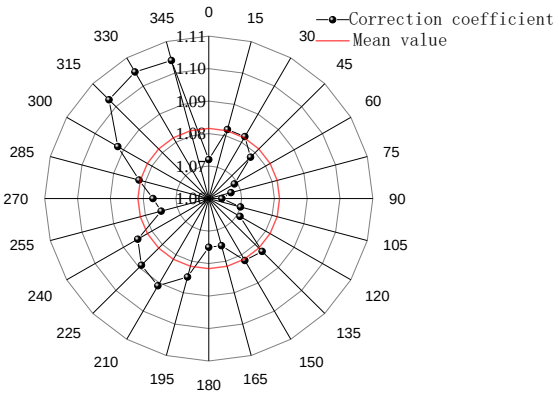

Fig. 7 Wind speed correction factors under different wind directions

Fig. 6 shows the wind speeds at the reference height under different wind angles for the return period from 10 to 50 years. The terrain correction factors at the reference height were calculated based on simulation of the terrain effect in the considered wind directions, as shown in Fig. 7. Radially, the terrain correction factor varied from 1.06 to 1.11, and the increment of coordinate was 0.01. The wind tunnel test indicated a prominent 3D terrain effect at the top of Xiushan Mountain and the terrain correction factors varied significantly at the reference height at different wind angles. The maximum terrain correction factor was 1.105, occurring at a wind angle of 330°. This means the most adverse wind speed acceleration occurred at 330° wind angle. However, the terrain correction factors estimated from the simulation were smaller than the results by the standard formula of 2D correction factor (1.193). Terrain factors had a considerable impact on wind force distribution of the television tower. Therefore, the following computation of ESWLs was based on the 3D terrain effect.

5. Results of force measurement experiment and analysis

5.1 Structural modes and computation parameters

Fig. 8 shows the changes of frequencies of the first 15

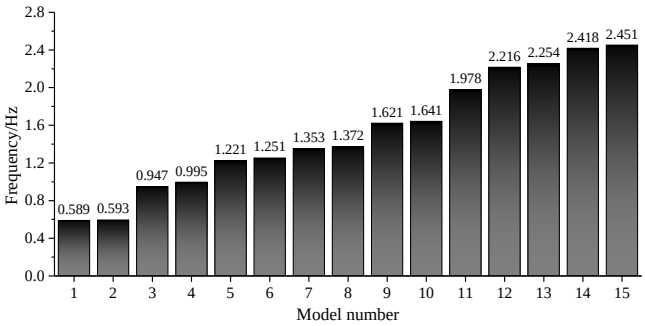

Fig. 8 Changes of frequency with mode order

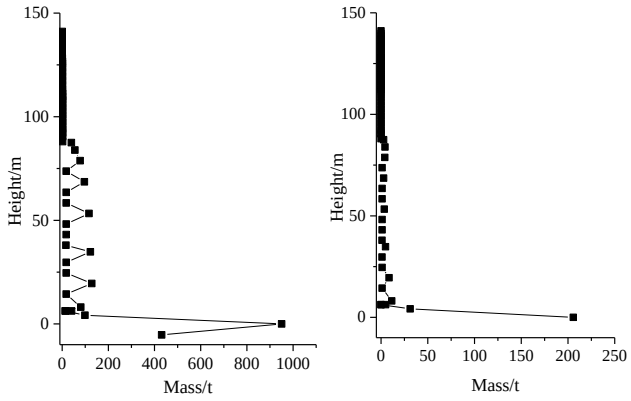

(a) Mass distribution (b) Rotational inertia distribution

Fig. 9 Distribution of mass and rotational inertia of each layer of tower

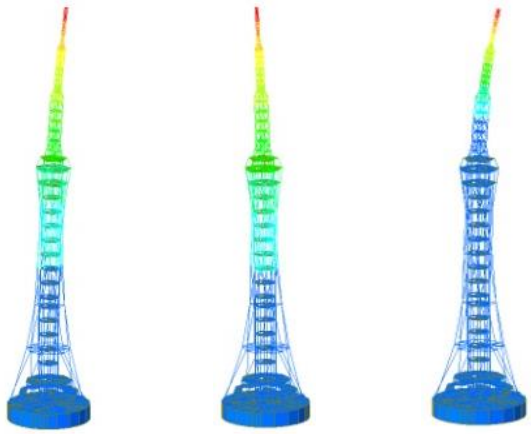

(a) First mode (b) Second mode (c) Third mode

Fig. 10 The first 3 modes of TV model

vibration mode orders. Figs. 9 and 10 show the distributions of mass and rotational inertia of the tower with height and the first 3 modes, respectively.

he natural periods of first 2 modes were 1.698s and 1.686s, respectively. The peak factor was taken as 2.5 and the modal damping ratio n as 2.0% and 3.5%, respectively. On this basis, ESWLs of the foundation and each layer were computed for the first 3 order modes. The contribution rates of each order mode are presented in Table 1.

Table 1 Contribution rates of the first 3 modes in different directions (%)

Mode	*X* axis	*Y* axis	*Z* axis
1	0.83	90.12	0.00
2	91.17	0.88	0.00
3	0.00	0.00	100.00

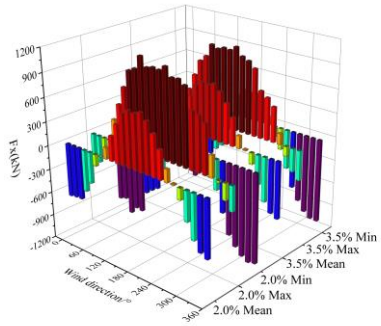

(a) Overturning moment around *X* axis

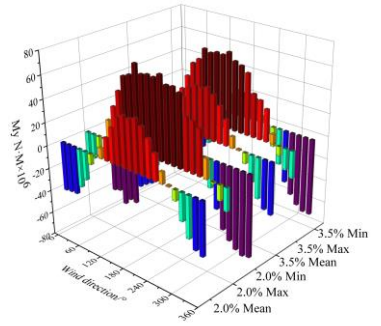

(b) Overturning moment around *Y* axis

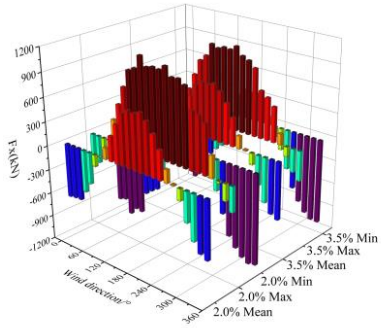

(c) Shear force around *X* axis

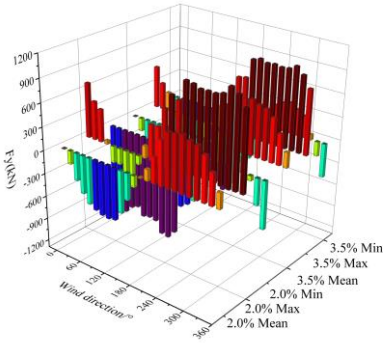

(d) Shear force around *Y* axis

Fig. 11 Curves of mean, maximum and minimum equivalent internal force of foundation

Table 2 Maximum absolute values of equivalent internal force of foundation and the corresponding angles

Damping ratio	Equivalent internal force of foundation and the corresponding wind angles							
	$\|F_x\|$max/N	Wind angle	$\|F_y\|$max/N	Wind angle	$\|M_x\|$max/(N·m)	Wind angle	$\|M_y\|$max/(N·m)	Wind angle
2.0%	1.155×106	135°	1.239×106	135°	7.859×107	135°	7.328×107	135°
3.5%	1.063×106	345°	1.117×106	120°	7.088×107	105°	6.744×107	330°

5.2 Internal force of foundation

Fig. 11 shows the curves of characteristic values of bending moments and shear strength (mean, maximum and minimum) at the foundation at a damping ratio of 2.0% and 3.5% for the return period of 50 years, respectively. The changes of internal force of foundation displayed a consistent pattern in different wind directions, which resembled a sine and cosine curves. At wind angle of 0° and 180° (across-wind in *Y* axis), the structure was affected by wind loads in a quasi-symmetrical way; the shear force F_y along *Y* axis and bending moment M_x along *X* axis were about 0. At wind angle of 90° and 270°, the absolute values of F_y and M_x reached the maximum. In contrast, at wind angle of 0° and 180°, the absolute values of shear force F_x along *X* axis and bending moment My along *Y* axis reached the maximum. At wind angle of 90° and 270°, F_x and M_y were about 0.

Table 2 shows the maximum absolute values of internal force of foundation. As the damping ratio increased, ESWLs of the foundation decreased and the across-wind loads were sensitive to the damping ratio. Under wind loads, the across-wind force and moment were non-negligible. Therefore, the structural design should not only consider the along-wind loads, but also the across-wind loads. At the wind angle of 135°, both the equivalent bending moment and internal force of the foundation reached the maximum, and this feature deserves extra attention in the subsequent computation of wind-induced vibration and structural design.

5.3 Peak acceleration response of the top of structure

According to national standards, the maximum accelerations along-wind and across-wind at the top of public buildings under the wind loads with a return period of 10 years should not exceed 0.28 m/s. Fig. 12 shows the components of acceleration response at the top of structure (excluding the antenna) at different damping ratios for the return period of 10 years. Table 3 shows the maximum acceleration response and the corresponding wind angles. Analysis showed that

1) At wind angle of 0° and 180°, the peak acceleration at the top of structure along *Y* axis was obviously higher than that along *X* axis; at wind angle of 90° and 270°, the peak acceleration at the top of structure along *X* axis was higher than that along *Y* axis;

2) The peak acceleration response at top of structure was greatly affected by wind angle. The extreme of acceleration response along *X* and *Y* axis showed a difference by 2.77 and 2.46 times, respectively. The reasons were two-fold: firstly, imperfect symmetry of internal tower structure;

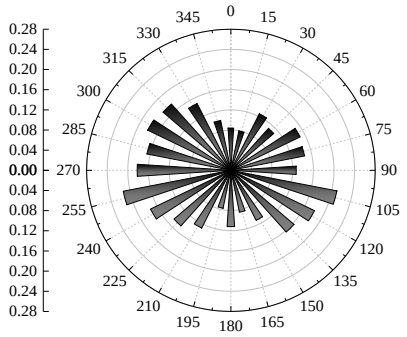

(a) n=2.0%, acceleration along *X* axis

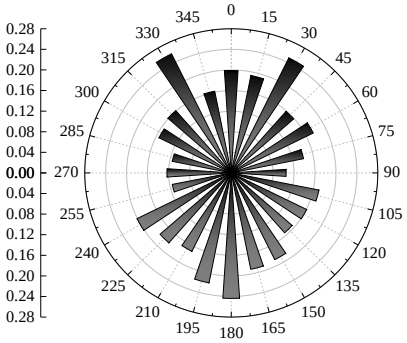

(b) n=2.0%, acceleration along *Y* axis

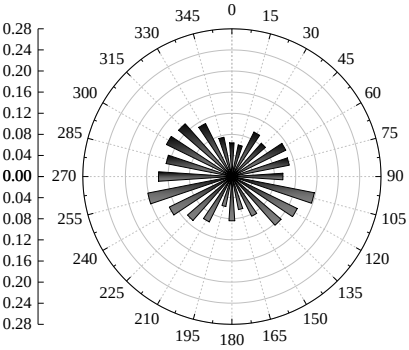

(c) =3.5%, acceleration along *X* axis

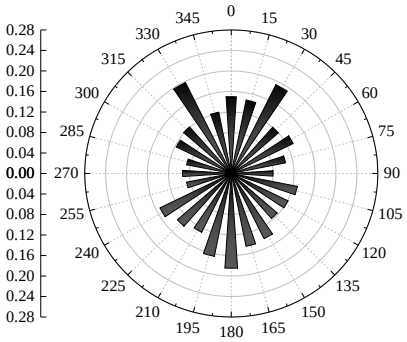

(d) n=3.5%, acceleration along *Y* axis

Fig. 12 Components of acceleration peak response of top of structure at different damping ratios

Table 3 Peak acceleration responses at top of the structure under different damping ratios and the corresponding wind angles

Damping ratio	Peak acceleration along X axis at top of structure		Peak acceleration along Y axis at top of structure	
	Value/m·s-2	Wind angle/°	Value /m·s-2	Wind angle /°
2.0%	0.213	255	0.258	330°
3.5%	0.161	255	0.198	330°

secondly, the 3D terrain effect.

3) None of the peak acceleration responses along X and Y axis exceeded the imposed limits. The maximum acceleration response (0.258 m/s^2) occurred along Y axis under 330° wind angle. This is believed to satisfy the comfort standards according to the analysis. But some researchers (Glanville and Kwok 1995, Zhang *et al*. 2001) showed that this peak acceleration is close to the value for tall television towers standing 400 m high.

6. Analysis of ESWLs

6.1 ESWLs for different layers of the tower

ESWLs under the same load conditions consist of loads along two primary directions. The ESWLs along these two directions will not reach the maximum simultaneously, and an empirical coefficient is generally used to determine the combination of loads along secondary direction. Considering the effect of the empirical coefficient on the components of ESWLs along X and Y axis (secondary direction), respectively, the formulas for determining the combination of loads at different layers along Y and X axis are given below, with the empirical coefficient taken as 0.4 (Ke and Wang 2016). The first combination takes the Y axis as the secondary direction

$$\begin{aligned} E_{x_1} &= M_{Fx} + \mathrm{sgn}(M_{Fx})GS_{Fx} \\ E_{y_1} &= M_{Fy} + 0.4\,\mathrm{sgn}(M_{Fy})GS_{Fy} \end{aligned} \tag{19}$$

The second combination takes the X axis as the secondary direction

$$\begin{aligned} E_{x_2} &= M_{Fx} + 0.4\,\mathrm{sgn}(M_{Fx})GS_{Fx} \\ E_{y_2} &= M_{Fy} + \mathrm{sgn}(M_{Fy})GS_{Fy} \end{aligned} \tag{20}$$

where E_{x1} and E_{y1} are the components of ESWLs in each layer along X and Y axis under the first combination, respectively; E_{x2} and E_{y2} are the components of ESWLs in each layer along X and Y axis under the second combination, respectively; G is peak factor; M_{Fx}, S_{Fx}, M_{Fy} and S_{Fy} are the means and variances of shear force F_x and F_y at the foundation, respectively.

Figs 13 and 14 show the schematic of 3D distribution of ESWLs in each layer under the two combinations, respectively. The distribution of components of ESWLs along X axis was symmetrical, and the distribution pattern varied significantly with wind angle. The peak platform of components along X axis under the second combination was

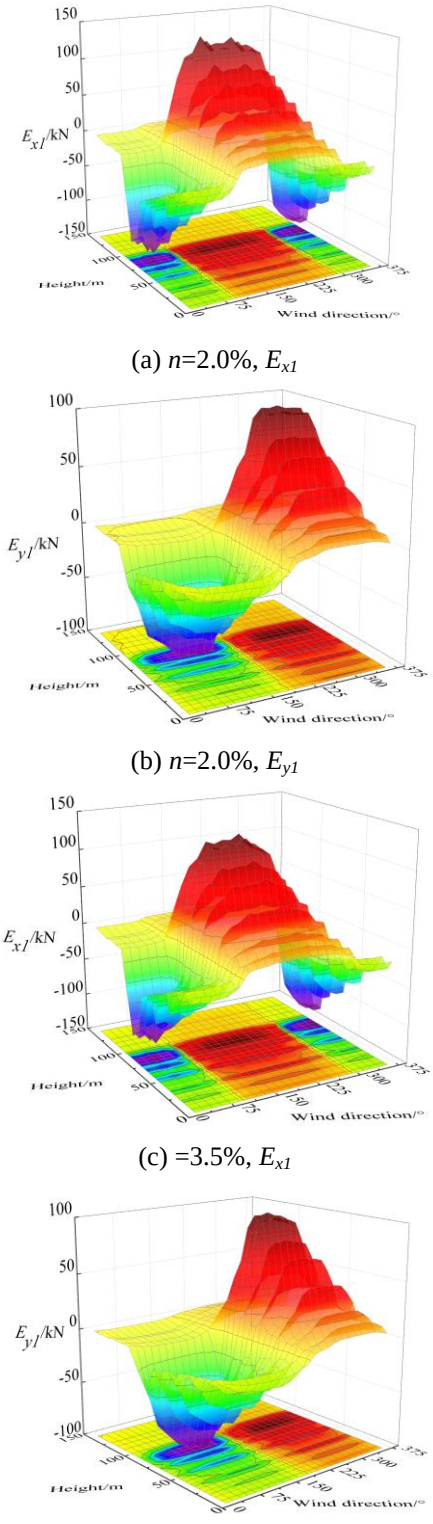

(a) n=2.0%, E_{x1}

(b) n=2.0%, E_{y1}

(c) =3.5%, E_{x1}

(d) n=3.5%, E_{y1}

Fig. 13 3D distributions of ESWLs of the tower under the first combination

obviously shorter as compared with that under the first combination; however, the situation was just the opposite along Y axis. The peak component of ESWLs along X axis was 140 kN under the first combination. At 2.0% damping ratio, the peak component of ESWLs along X axis was only

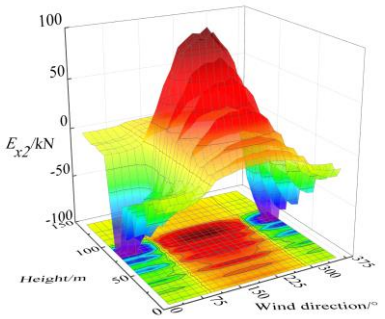

(a) n=2.0%, E_{x1}

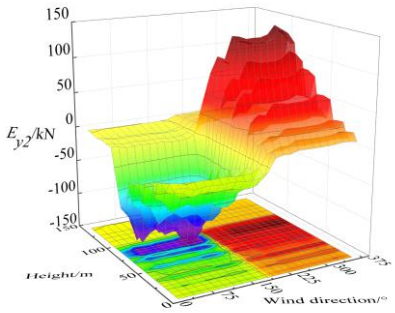

(b) n=2.0%, E_{y1}

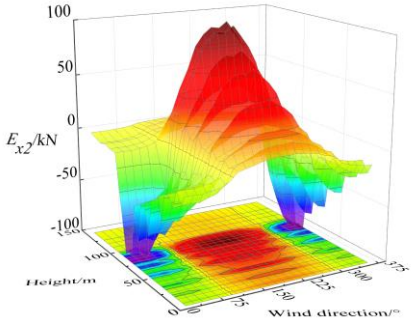

(c) =3.5%, E_{x1}

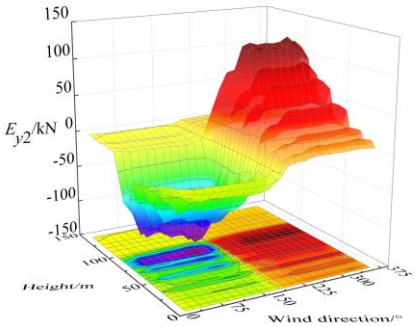

(d) n=3.5%, E_{y1}

Fig. 14 3D distributions of ESWLs of the tower under the second combination

106 kN under the second combination. The variations of ESWLs with height were little affected by load combinations or wind angle.

6.2 ESWLs under the most adverse wind angle

Distributions of each component of ESWLs with height

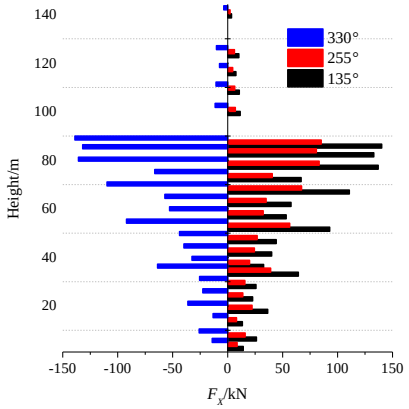

(a) n=2.0%, F_x components

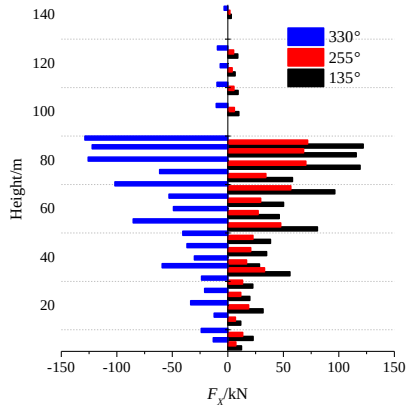

(b) n=3.5%, F_x components

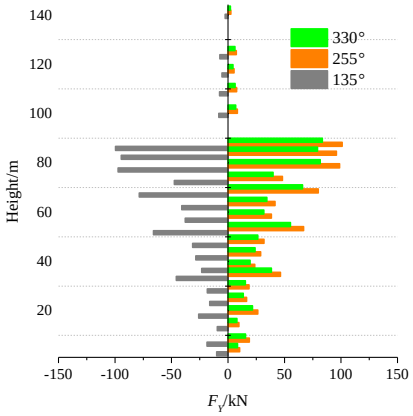

(c) n=2.0%, F_y components

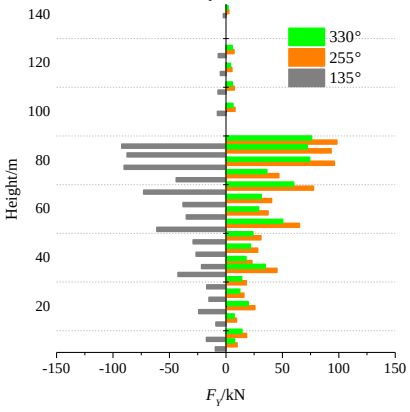

(d) n=3.5%, F_y components

Fig. 15 Distributions of ESWLs with height under the most adverse wind angles and different damping ratios

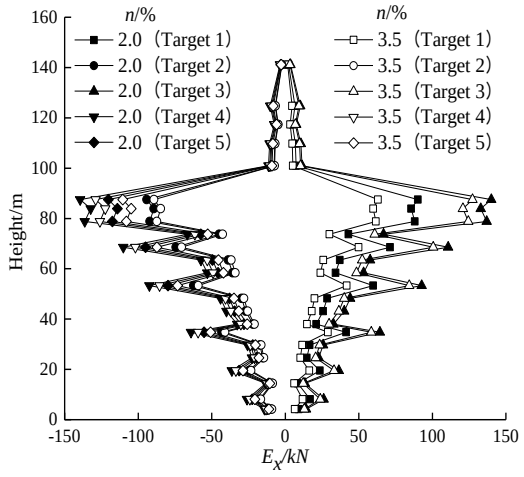

(a) n=2.0%, F_x components

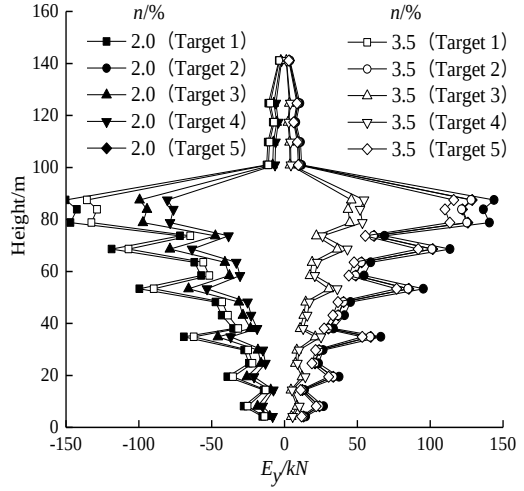

(b) n=3.5%, F_x components

Fig. 16 Schematic of changes of ESWLs with height under different load conditions

at different damping ratios for the three most adverse wind angles (135°, 255° and 330°) were showed in Fig. 15. The following conclusions were arrived at:

1) ESWLs at each layer of the television tower under 135° wind angle were higher than those at other adverse wind angles;

2) At 255° wind angle where the peak acceleration occurred at the top of structure along X axis, the component along X axis was smaller in the main tower. At 330° wind angle where the peak acceleration occurred at the top of structure along Y axis, the component along Y axis was smaller in the main tower.

3) Under the three most adverse wind angles, ESWLs increased with height in the main tower. In contrast, the ESWLs of the antenna mast decreased with height.

6.3 ESWLs under specific load conditions

The choice of combination coefficient was based on load conditions. ESWLs of each layer were computed under 5 load conditions with n=2.0% and 3.5%, respectively. The equivalent goals were: 1) maximum bending moment around X axis; 2)minimum bending moment around X axis; 3) maximum bending moment around Y axis; 4)minimum bending moment around Y axis; 5)maximum square roots of sum of squares of bending moment in 2 directions.

Fig. 16 shows the curves of ESWLs with height under 5 load conditions. It can be seen that the distribution patterns of ESWLs with height were consistent, with the maximum ESWLs found at the top of main tower. ESWLs for each layer varied significantly under different load conditions. For example, under load condition 3, the peak E_x was 140 kN; under load condition 1, the peak E_x was only 90 kN. Damping ratio had a significant impact on ESWLs of the main tower, while the impact from the equivalent goals and damping ratio on ESWLs of the antenna mast was less significant. Given the considerable flexibility and whiplash effect of the antenna mast, check computation of ESWLs for each layer is necessary.

7. Conclusions

This study focused on the impact of terrain factors of hilltops, wind-induced vibration and distribution features of ESWLs in the design of tall television towers. Simulation of terrain effect by wind tunnel test, force measurement experiment, finite element analysis, technique for determining load combinations and parametric analysis were performed. The research presented in this paper has resulted in the following:

1) Simulation of the terrain effect indicated a salient 3D distribution feature. The most adverse wind speed acceleration occurred at 330° wind angle. The terrain correction factors under different wind directions estimated by simulation were smaller than the single values provided in the national standard. For mountainous regions, the 3D terrain effect should be considered in wind speed correction.

2) Internal force of foundation and the peak accelerations at the top of structure were significantly influenced by the wind angle of the incoming flow. The most adverse wind angles were 135° and 330°. Due to terrain effect, the peak acceleration, which was 0.258 m/s^2, far exceeded the value for the television towers of the same height; moreover, the internal force and moment of force across-wind were non-negligible.

3) ESWL distributions in each layer of the tower were very distinct in different directions in 3D space. The distribution of ESWLs of the main tower was little affected by wind angle, damping ratio and equivalent goals and the values increased with height; the maximum ESWL occurred at 135° wind angle. In contrast, for the antenna mast, ESWLs decreased with height.

4) Using the improved technique for determining load combinations for ESWLs, parametric analysis of ESWLs under different equivalent goals were performed, and ESWLs of the tower under 5 typical load conditions were derived, too. The above findings provide reference for determining wind loads for tall television towers built on hilltops.

Acknowledgments

The research is jointly supported by National Natural Science Foundation (51208254 and 51021140005), Jiangsu Province Outstanding Natural Science Foundation (BK20160083), and Postdoctoral Science Foundation (2013M530255; 1202006B), which are gratefully acknowledged

References

American Standards (2010), "Minimum Design Loads for Buildings and Other Structures", ASCE 7-10, Structural Engineering Institute

Belloli, M., Rosa, L. and Zasso, A. (2014), "Wind loads on a high slender tower: Numerical and experimental comparison", *Eng. Struct.*, **68**(4), 24-32.

Breuer, P., Chmielewski, T., Górski, P., Konopka, E. and Tarczyński, L. (2008), "The Stuttgart TV Tower-displacement of the top caused by the effects of sun and wind", *Eng. Struct.*, **30**(10), 2771-2781.

Carril, C.F., Isyumov, N. and Brasil, R.M.L.R.F. (2003), "Experimental study of the wind forces on rectangular latticed communication towers with antennas", *J. Wind Eng. Indust. Aerodyn.*, **91**(8), 1007-1022.

Chinese Standards (2012), "Lode Code for The Design of Building Structures", GB50009-2012, China Building Industry Press. (in Chinese)

Feng, M.Q. and Zhang, R. (1997), "Wind-induced vibration characteristics of Nanjing TV tower", *Int. J. Nonlin. Mech.*, **32**(4), 693-706.

Glanville, M.J. and Kwok, K.C.S. (1995), "Dynamic characteristics and wind induced response of a steel frame tower", *J. Wind Eng. Indust. Aerodyn.*, **54-55**(2), 133-149.

Japanese Standards (2004), "AIJ Recommendations for Loads on Buildings", AIJ 2004, Research Committee on Structures. (in Japanese).

Kareem, A. and Kabat, S., Jr F.L.H. (1997), "Aerodynamics of Nanjing Tower: a case study", *J. Wind Eng. Indust. Aerodyn.*, **77-78**(5), 725-739.

Ke, S.T. and Wang, H. (2016), "Analysis on equivalent static wind loads of large television tower considering topographic effect", *J. Southeast Univ. Nat. Sci. Ed.*, **46**(3), 545-551. (in Chinese)

Ke, S.T., Ge, Y.J., Zhao, L. and Tamura, Y. (2012), "A new methodology for analysis of equivalent static wind loads on super-large cooling towers", *J. Wind Eng. Indust. Aerodyn.*, **111**(111), 30-39.

Ke, S.T., Wang, T.G., Ge, Y.J. and Tamura, Y. (2014), "Wind-induced responses and equivalent static wind loads of tower-blade coupled large wind turbine system", *Struct. Eng. Mech.*, **52**(3), 485-505

Kitagawa, T., Wakahara, T., Fujino, Y. and Kimura, K. (1997), "An experimental study on vortex-induced vibration of a circular cylinder tower at a high wind speed", *J. Wind Eng. Indust. Aerodyn.*, **69**(3), 731-744.

Li, B., Yang, Q. and Yang, J. (2016), "Wind characteristics near ground in south-eastern coast area of China based on field measurement", *Geomat. Nat. Hazard. Risk*, **3**(4), 1-13.

Li, Z.L, Wei, Q.K., Huang, H.J. and Sun, Y. (2011), "Wind-induced response of super tall building in hilly terrain", *J. Vib. Shock*, **30**(5), 43-48.

Pirner, M. and Fischer, O. (1999), "Long-time observation of wind and temperature effects on TV towers", *J. Wind Eng. Indust. Aerodyn.*, **79**(1), 1-9

Simiu, E. and Scanlan, R.H. (1978), *Wind Effects on Structures: an Introduction to Wind Engineering*, Wiley

Yang, F., Dang, H. and Niu, H. (2016), "Wind tunnel tests on wind loads acting on an angled steel triangular transmission tower", *J. Wind Eng. Indust. Aerodyn.*, **156**(156), 93-103.

Zhang, Z.Q., Li, A.Q. and Can, D.Y. (2016), "Simulation of dynamic wind load on Heifei Television Tower", *J. Southeast Univ. Nat. Sci. Ed.*, **31**(1), 69-73. (in Chinese)

Zhou, X., Huang, P. and Gu, M. (2010), "Wind loads and wind-induced responses of guangzhou new TV tower", *Adv. Struct. Eng.*, **13**(4), 707-726.

CC